

## Finite strip analysis of multi-span box girder bridges by using non-periodic B-spline interpolation

C.K. Choi<sup>†</sup>

*Department of Civil Engineering, KAIST, Daejeon 305-701, Korea*

H.S. Hong<sup>‡</sup>

*Structural Division, Chungbuk Engineering Co., Seoul 137-809, Korea*

**Abstract.** A multi-span bridge has the peak value of resultant girder moment or membrane stress at the interior support. In this paper, the spline finite strip method (FSM) is modified to obtain the more appropriate solution at the interior support where the peak values of solution exist. The modification has been achieved by expressing the shape function with non-periodic B-splines which have multiple knots at the boundary. The modified B-splines have the useful feature for interpolating the curve with sudden change in curvature. Moreover, the modified spline FSM is very efficient in analyzing multi-span box girder bridges, since a bridge can be modeled by an assembly of strips extended along the entire bridge length. Numerical examples of the bridge analysis have been performed to verify the efficiency and accuracy of the new spline FSM.

**Key words:** finite strip; non-periodic B-spline function; multi-span bridge.

---

### 1. Introduction

The spline finite strip method (FSM) is very efficient for the analysis of bridges with constant geometrical properties, such as box girder bridges. In the spline FSM, the displacement field is constructed by using cubic(B3)-spline interpolation in the longitudinal direction and standard polynomial interpolation in the transverse direction. Cheung (1983) was the first to use the spline FSM for box girder bridge analysis. Recently, the isoparametric spline FSM was developed for shell analysis (Au and Cheung 1995) and applied to the static and free vibration analysis of variable-depth bridges of arbitrary alignments (Cheung and Au 1996).

On the other hand, the modeling of engineering problems frequently requires the restraint of a number of interior nodes. The introduction of these restraints in standard B3-spline formulation is a very cumbersome task. The reason for this is that the primary variables in a B3-spline interpolation are displacement parameters rather than real displacements and the shape function does not satisfy the Kronecker delta properties at that boundary. The real displacement at a section knot is a function of the nodal parameters of several adjacent knots. Therefore, retaining a section knot

---

<sup>†</sup> Institute Chair Professor

<sup>‡</sup> Ph.D., Vice-director

(making its nodal parameter zero) will not always result in zero displacement at that knot. Researchers have tried to overcome this problem by applying special treatments such as modified B3-splines and transformation procedures which change the displacement parameters into real displacements (Uko and Cusens 1988). It has been found that the use of this approach destroys the bandedness of the system and results in a full stiffness matrix which significantly reduces the computational efficiency. Moreover, the magnitude and direction of end tangential vectors are also required in order to approximate the geometry of a structure in the case of the isoparametric spline FSM (Cheung and Au 1995). Thus, a more efficient analysis method for continuous box girder bridges by the isoparametric spline FSM is yet to be developed. The improved FSM should provide more accurate stress evaluation, simpler input/output processes, and the reduction of DOF.

As the main strategy to achieve this goal in the present paper, the standard B3-splines are modified to be non-periodic B3-splines which satisfy the Kronecker delta properties at the boundary. The non-periodic B3-splines are used for the displacement function and also for the description of geometry in the formulation of an isoparametric spline FSM. This interpolation makes it possible to introduce interior supports at any location in much the same way as in the standard finite element formulation while the bandedness of the method is retained. The accuracy and efficiency of the proposed FSM have been verified for the case of multi-span box girder bridge analysis.

## 2. Non-periodic B-spline representation

### 2.1 Determination of shape function

The previous use of periodic B-spline function for the analysis of multi-span bridges (Au and Cheung 1996) is limited to the interpolation of smooth curves. When the profile of a bridge includes a sudden break in slope or curvature along its length, the bridge has to be divided into several substructures for analysis, making the process of automatic input or modeling difficult.

To solve the problem mentioned above, the use of non-periodic B-spline functions is proposed as an efficient method for the analysis of multi-span bridges. If a B3-spline series has repeated knot vector values at the boundary point, the extra spans beyond the end points all have zero lengths, and thus both initial and final knots become multiple knots (Fig. 1) with a multiplicity of 4 (order of B3-spline). Thus the B3-spline series has been modified to become a non-periodic B3-spline series. In the non-periodic B3-spline series, the use of multiple knots at the boundaries enables the Kronecker delta property to be satisfied and thus the real values of the field variables, not parameters, can be directly obtained at the boundary. Therefore, the boundary conditions can be treated more easily.

In Fig. 1(b), it can be found that the non-periodic B3-spline series have multiple knots of 4 at knots  $T_0$  and  $T_n$  and thus, B3-splines at both ends  $\phi_{-1}$ ,  $\phi_{n+1}$  have only two knot vector positions. Except at the ends (or boundaries), the remaining knots are aligned to be equally spaced along the longitudinal direction (Fig. 1).

The non-periodic B-spline function is defined by the recursive form expressed as

$$B_{i,1}(t) = \begin{cases} 1 & \text{for } T_i \leq t \leq T_{i+1} \\ 0 & \text{otherwise} \end{cases} \quad (1a)$$

and

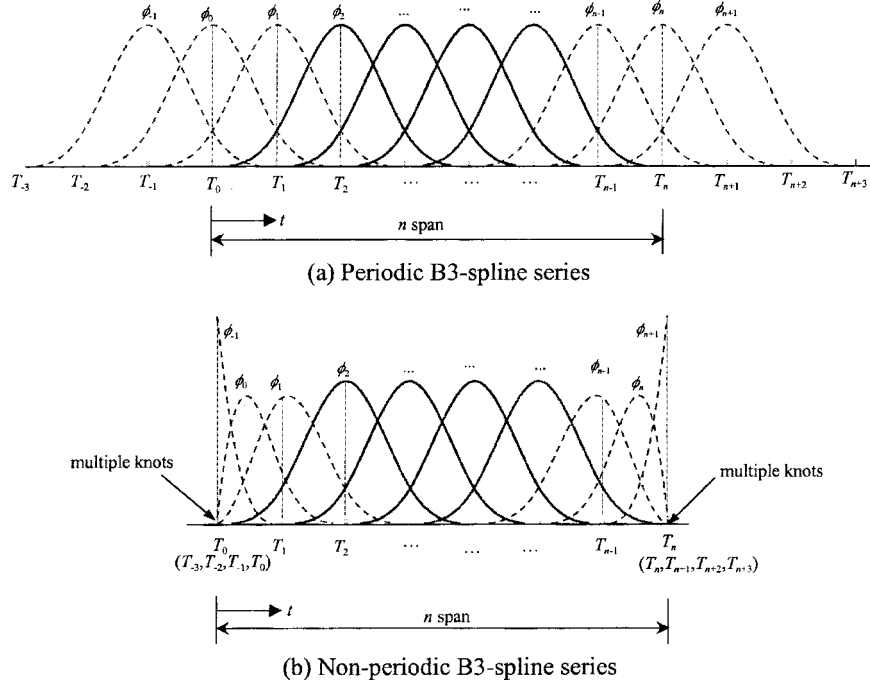


Fig. 1 Periodic B3-spline series and non-periodic B3-spline series

$$B_{i,k}(t) = \frac{(t - T_i)}{(T_{i+k-1} - T_i)} B_{i,k-1}(t) + \frac{(T_{i+k} - t)}{(T_{i+k} - T_{i+1})} B_{i+1,k-1}(t) \quad \text{for } k \geq 2 \quad (1b)$$

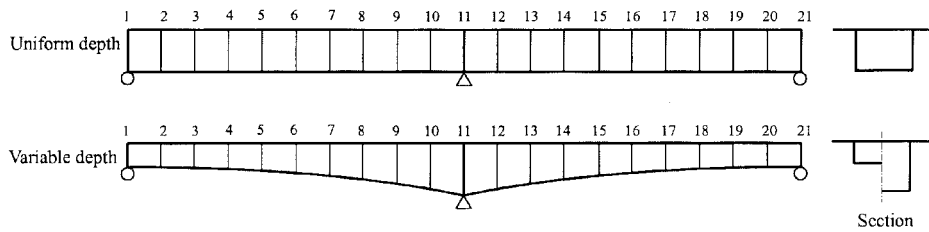
where,  $(T_i, \dots, T_{i+k})$  are the knot vectors. For convenience, let  $\phi_i = B_{i-2,4}$  in the expressions hereafter. By substituting multiple knot values  $T_i$ s into Eq. (1) at an end (or boundary), the non-periodic B-spline series can be established easily. The non-periodic B-splines  $\phi_i$  retain the  $C^{k-2}$  continuity property and the partition of unity property, and thus these B-splines can also be used as the shape function.

Fig. 2 illustrates the profile of two-span box girder bridges with 20 sections defined by 21 nodes in the longitudinal direction and the 21 associated B3-spline series with multiple knots at the boundaries, evaluated by using the recursive relation (Eq. 1). Due to the knot multiplicities at the end supports and the interior support, these 21 B3-spline series need to have only 17 knot positions (16 spans) to be defined.

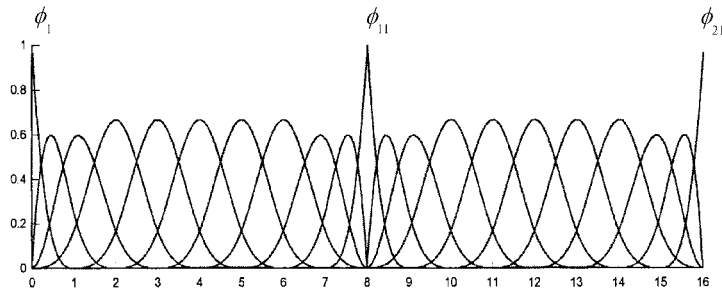
The displacement field can be approximated by the shape function and displacement parameters. The shape function is constructed by the multiplication of transverse shape functions  $L_j$  (Lagrange polynomials) and the non-periodic B3-splines  $\phi_i$  in the longitudinal direction as

$$\mathbf{u} = \sum_{i=-1}^{n+1} \sum_{j=1}^2 N_{ij}(\xi, \eta) \mathbf{a}_{ij} = \sum_{i=-1}^{n+1} \sum_{j=1}^2 L_j(\xi) \phi_i(\eta) \mathbf{a}_{ij} \quad (2)$$

where,  $\mathbf{a}_{ij}$  denotes the displacement parameter of the  $j$ -th nodal line and  $i$ -th nodes(not knots) in the longitudinal direction. Here, the real displacement of a nodal line can be represented by the displacement parameter of the nodal line and the non-periodic B3-spline function.



(a) Continuous bridges with uniform(constant) depth and variable depth

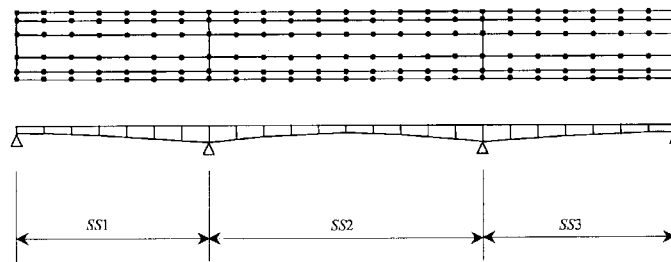


(b) B3-spline series with multiple knots at boundary

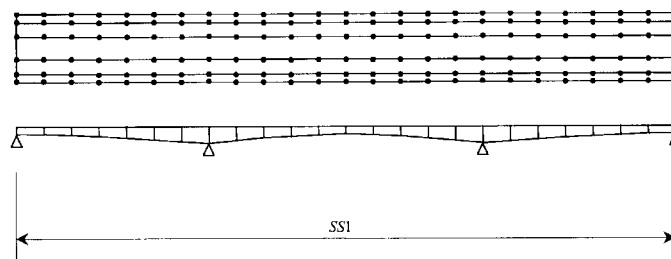
Fig. 2 Profile of continuous bridge and associated B3-spline series

2.2 Geometric description of bridge

For the finite strip modeling of continuous variable depth bridges, the conventional FSM uses the



(a) Conventional spline finite strip(three strips)



(b) Proposed spline finite strip(single strip)

Fig. 3 Typical three-span bridges and schemes for sub-division

periodic B3-spline as a component of the shape function. As shown in Fig. 3, the variable depth bridge has a break in curvature at the interior supports and the periodic B3-spline function has the severe restriction in interpolating the non-smooth curve. Therefore, continuous(multi-span) bridges with variable depth have to be divided into several substructures for analysis. As shown in Fig. 3(a), three substructures should be used for the bridge in the conventional periodic spline finite strip method and therefore, the automatic modeling may not be possible.

However, the proposed non-periodic B3-spline representation can express the peak values at supports (also discussed in Sec3.1) and effectively interpolate the geometry of a three-span bridge with variable depth by using only a single strip along the entire bridge length as shown in Fig. 3(b). Thus modeling multi-span bridges by the non-periodic B3-spline is simpler and more efficient when compared with the conventional periodic B3-spline. Moreover, the capability of non-periodic B3-spline representation to express the peak values at the interior supports is most suitable for expressing the peak negative moments of the bridge which may not be appropriately expressed by other methods, e.g., the finite element method.

### 3. Formulation of non-periodic finite strip

#### 3.1 Geometry definition of strip and local axis

A typical finite strip can be generated by dividing an arbitrary shell (plate) into several strips. Each strip has  $n$  sections (or  $n+1$  interior nodes) and each nodal line between two strips is defined by a curve defining a polygon of  $(n+1)$  vertices. Even though the strip may have a non-smooth surface including sharp edges, the geometry of a strip can be interpolated by a single non-periodic finite strip along the longitudinal direction (Fig. 4).

The geometry of the  $C^0$  degenerated shell strip of general shape is defined in terms of functions of the mid-surface only (Kebari and Cassell 1991) by

$$\mathbf{x} = \sum_{i=1}^{n+1} \sum_{j=1}^2 N_{ij}(\xi, \eta) \mathbf{q}_{ij} + t \mathbf{V}_t \tag{3}$$

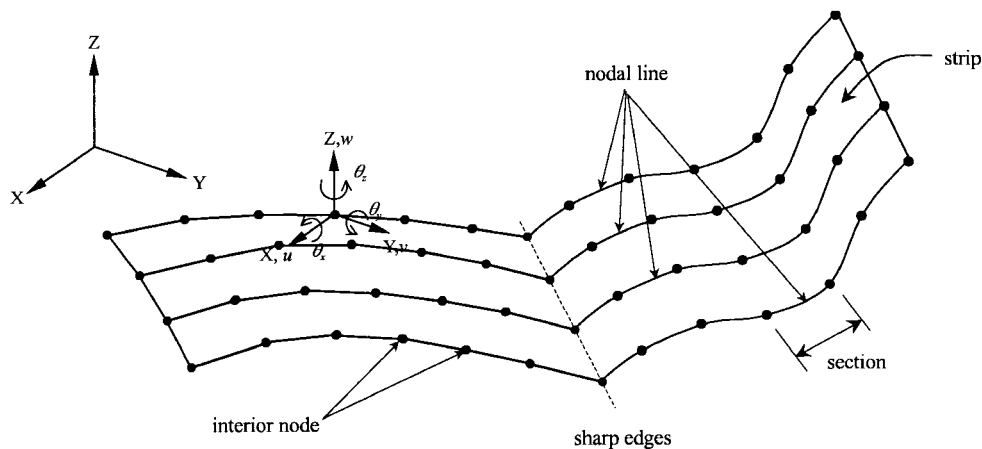


Fig. 4 Strip geometry with sharp edge and coordinates system

where  $\mathbf{x}=(x, y, z)$  is the position vector of shell geometry and  $N_{ij}$  is a shape function defined in Eq. (2).  $\mathbf{V}_t$  is the unit vector normal to the shell mid-surface at each integration point,  $t$  is the linear coordinate in the range  $-h/2 < t < h/2$  and  $h$  is the thickness at the integration point.  $\mathbf{q}_{ij}$  is the  $i$ -th curve defining vector of the  $j$ -th nodal line of the strip.

In order to obtain the curve defining vector  $\mathbf{q}_{ij}$ , the inverse of the parametrization matrix should be obtained (Farin 1992). In the case of uniform B3-splines, a smooth curve with  $n$  sections should be defined with  $(n+3)$  curve defining vectors. Therefore, the parametrization matrix consists of  $(n+1)$  internal node position vectors and the tangential vectors at both ends of a nodal line (Au and Cheung 1995).

In the non-periodic B-spline finite strip method, the geometry (or spline curve) can be evaluated using the non-periodic B3-splines by only  $(n+1)$  internal node position vectors without any tangential vectors due to the multiple knots. In this study, the interior nodes are assumed to be located in a uniform spacing in the longitudinal direction and the parametrization matrix is made from only  $(n+1)$  internal node position vectors.

Fig. 5(a) shows that the non-periodic spline curve can be evaluated by only  $(n+1)$  internal node position vectors. Especially, as shown in Fig. 5(b), the non-periodic B3-spline function can be effectively used to describe the geometry of continuous bridge with variable depth by an assembly of non-segmented longitudinal strips.

The covariant natural-coordinate unit vectors are then obtained by:

$$\mathbf{V}_\xi = \frac{1}{A_\xi} \frac{\partial \mathbf{x}}{\partial \xi} = \frac{1}{A_\xi} \begin{Bmatrix} x,\xi \\ y,\xi \\ z,\xi \end{Bmatrix}, \quad \mathbf{V}_\eta = \frac{1}{A_\eta} \frac{\partial \mathbf{x}}{\partial \eta} = \frac{1}{A_\eta} \begin{Bmatrix} x,\eta \\ y,\eta \\ z,\eta \end{Bmatrix} \quad (5)$$

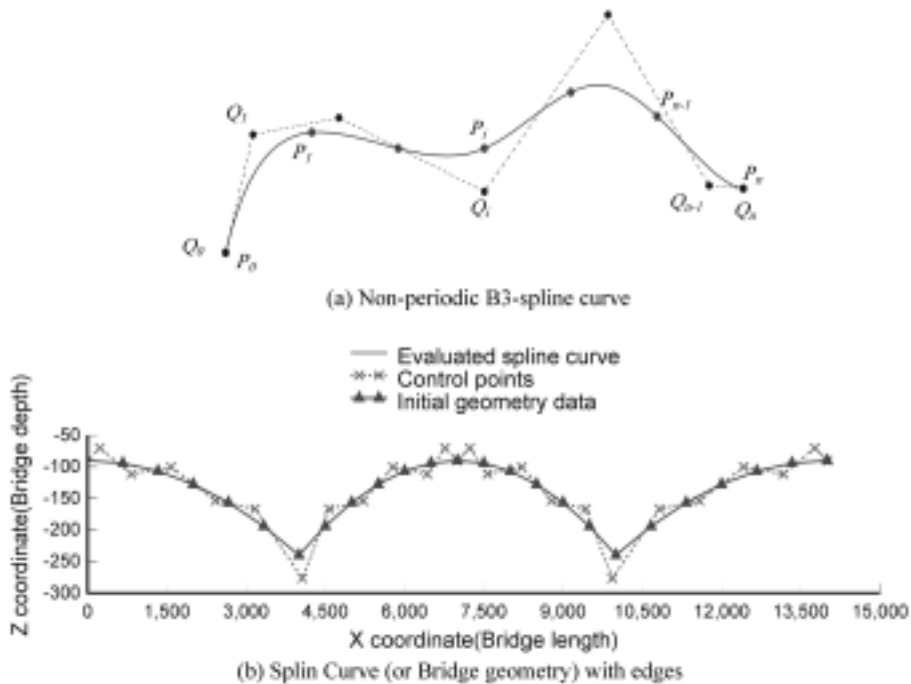


Fig. 5 Non-periodic B3-spline curves

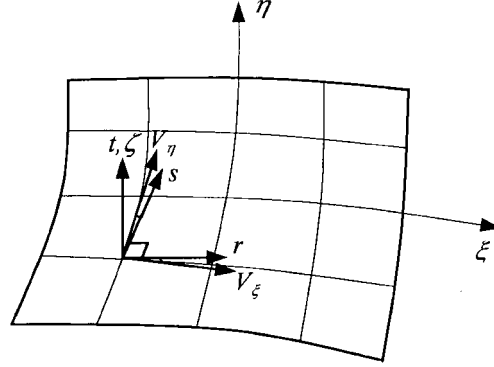


Fig. 6 Local coordinate system at the integration point

where

$$A_{\xi} = |\mathbf{x}_{,\xi}| = (\mathbf{x}_{,\xi} \cdot \mathbf{x}_{,\xi})^{\frac{1}{2}}, \quad A_{\eta} = |\mathbf{x}_{,\eta}| = (\mathbf{x}_{,\eta} \cdot \mathbf{x}_{,\eta})^{\frac{1}{2}} \quad (6)$$

The mid-surface of the shell is described by two non-dimensional curvilinear coordinates  $\xi$ ,  $\eta$  and the axis  $\zeta$  is normal to the shell mid-surface. A local orthogonal coordinate system  $(r, s, t)$  at the integration point is constructed, such that  $(r, s)$  is symmetric with respect to the unit tangential vectors  $\mathbf{V}_{\xi}$ ,  $\mathbf{V}_{\eta}$  (Fig. 6). As shown in Fig. 6, the surfaces of the unit tangent vectors  $\mathbf{V}_{\xi}$ ,  $\mathbf{V}_{\eta}$  to the  $(\xi, \eta)$  and  $(r, s)$  surface are coplanar at the shell mid-surface. Naturally, the out-of-plane coordinates  $\zeta$  and  $t$  coincide. The orthogonal unit vectors  $\mathbf{V}_r$ ,  $\mathbf{V}_s$ ,  $\mathbf{V}_t$  parallel to the local coordinate axes  $(r, s, t)$  are established as follows:

$$\mathbf{V}_t = \frac{\mathbf{V}_{\xi} \times \mathbf{V}_{\eta}}{|\mathbf{V}_{\xi} \times \mathbf{V}_{\eta}|} = \begin{Bmatrix} l_3 \\ m_3 \\ n_3 \end{Bmatrix}, \quad \mathbf{V}_s = \frac{(\mathbf{V}_t \times \mathbf{V}_{\xi}) + \mathbf{V}_{\eta}}{|(\mathbf{V}_t \times \mathbf{V}_{\xi}) + \mathbf{V}_{\eta}|} = \begin{Bmatrix} l_2 \\ m_2 \\ n_2 \end{Bmatrix}, \quad \mathbf{V}_r = \mathbf{V}_s \times \mathbf{V}_t = \begin{Bmatrix} l_1 \\ m_1 \\ n_1 \end{Bmatrix} \quad (7)$$

### 3.2 Displacement and strain field

The kinematic variables are interpolated over the mid-surface of the strip using the two-dimensional interpolations. Six degrees of freedom per node are considered in the formulation of stiffness matrices and load vectors of the general shell finite strip element based on independent rotational and translational displacement interpolations. They are the three translational DOFs  $u, v, w$  and three rotational DOFs about the global axes (Fig. 4). The displacement vector for a typical point in the shell strip is introduced as follows

$$\mathbf{u} = \sum_{i=1}^{n+1} \sum_{j=1}^2 N_{ij} \mathbf{u}_{ij} + \sum_{i=1}^{n+1} \sum_{j=1}^2 N_{ij} \hat{\mathbf{u}}_{ij} \quad (8)$$

where

$$\hat{\mathbf{u}} = \begin{Bmatrix} \hat{u} \\ \hat{v} \\ \hat{w} \end{Bmatrix} = \frac{\zeta h}{2} \begin{bmatrix} 0 & n_3 & -m_3 \\ -n_3 & 0 & l_3 \\ m_3 & -l_3 & 0 \end{bmatrix} \begin{Bmatrix} \theta_x \\ \theta_y \\ \theta_z \end{Bmatrix} \quad (9)$$

$\mathbf{u}$  denotes the displacement of the shell mid-surface and  $\hat{\mathbf{u}}$  denotes the displacement of a fiber relative to the mid-surface.

In this study, adopting the conventional explicit integration through the thickness, the generalized strain-displacement relationships for a resultant stress shell strip are established as

$$\boldsymbol{\varepsilon}_m = \begin{Bmatrix} \boldsymbol{\varepsilon}_r \\ \boldsymbol{\varepsilon}_s \\ \boldsymbol{\varepsilon}_{rs} \end{Bmatrix} = \begin{Bmatrix} u_{r,r} \\ u_{s,s} \\ u_{r,s} + u_{s,r} \end{Bmatrix} = \mathbf{B}_m \mathbf{a} \quad (10a)$$

$$\boldsymbol{\varepsilon}_b = \begin{Bmatrix} \boldsymbol{\kappa}_r \\ \boldsymbol{\kappa}_s \\ \boldsymbol{\kappa}_{rs} \end{Bmatrix} = \begin{Bmatrix} \theta_{s,r} \\ -\theta_{r,s} \\ \theta_{s,s} - \theta_{r,r} \end{Bmatrix} = \mathbf{B}_b \mathbf{a} \quad (10b)$$

$$\boldsymbol{\varepsilon}_s = \begin{Bmatrix} \boldsymbol{\gamma}_{rt} \\ \boldsymbol{\gamma}_{st} \end{Bmatrix} = \begin{Bmatrix} u_{t,r} + \theta_s \\ u_{t,s} - \theta_r \end{Bmatrix} = \mathbf{B}_s \mathbf{a} \quad (10c)$$

where

$$\mathbf{a} = \sum_{j=1}^2 (\mathbf{a}_{1j}, \mathbf{a}_{2j}, \dots, \mathbf{a}_{n+1j}), \quad \mathbf{a}_{ij} = (\mathbf{u}_{ij}, \boldsymbol{\theta}_{ij}) \quad (11a)$$

$$\mathbf{u}_{ij} = (u_{ij} \ v_{ij} \ w_{ij})^T, \quad \boldsymbol{\theta}_{ij} = (\theta_{xij} \ \theta_{yij} \ \theta_{zij})^T \quad (11b)$$

and

$$\mathbf{B}_m = \begin{bmatrix} N_{ij,r} \mathbf{V}_r^T & \mathbf{0} \\ N_{ij,s} \mathbf{V}_s^T & \mathbf{0} \\ N_{ij,r} \mathbf{V}_s^T + N_{ij,s} \mathbf{V}_r^T & \mathbf{0} \end{bmatrix}, \quad \mathbf{B}_b = \begin{bmatrix} \mathbf{0} & N_{ij,r} \mathbf{V}_s^T \\ \mathbf{0} & -N_{ij,s} \mathbf{V}_r^T \\ \mathbf{0} & N_{ij,s} \mathbf{V}_s^T - N_{ij,r} \mathbf{V}_r^T \end{bmatrix}, \quad \mathbf{B}_s = \begin{bmatrix} N_{ij,r} \mathbf{V}_t^T & N_{ij} \mathbf{V}_s^T \\ N_{ij,s} \mathbf{V}_t^T & -N_{ij} \mathbf{V}_r^T \end{bmatrix} \quad (12)$$

### 3.3 Stiffness matrix by selectively reduced integration

The total potential energy of the elastic shell strip is given in two independent parts; the potential energy  $\Pi$  associated with three displacements and two local rotations

$$\Pi = \frac{1}{2} \int (\boldsymbol{\varepsilon}_m^T \mathbf{D}_m \boldsymbol{\varepsilon}_m + \boldsymbol{\varepsilon}_b^T \mathbf{D}_b \boldsymbol{\varepsilon}_b + \boldsymbol{\varepsilon}_s^T \mathbf{D}_s \boldsymbol{\varepsilon}_s) dA - W \quad (13)$$

and that with the drilling DOF  $\Pi_\theta$ .

$$\Pi_\theta = \Phi Gh \frac{1}{2} \int \varepsilon_\theta^T \varepsilon_\theta dA \quad (14)$$

where  $W$  is the potential energy of applied load,  $\Phi$  is a penalty constant, and the rigidity matrices  $\mathbf{D}_m$ ,  $\mathbf{D}_b$ ,  $\mathbf{D}_s$  are associated with membrane, bending and transverse shear strain, respectively. Further, an exact definition of drilling rotation in continuum mechanics is used as a constraint by the penalty function method: thus

$$\varepsilon_\theta = \theta_t - 1/2(u_{s,r} - u_{r,s}) = 0 \quad (15)$$

In this study,  $\Phi$  is chosen as 1.0 based on the test results of Choi and Hong (2001).  $\theta_t$  is the drilling rotation of the shell mid-surface in the local coordinate system defined as before.

By the principle of the stationary potential energy for equilibrium, the membrane, bending, and shear contributions to the total stiffness matrix for a strip are derived as

$$\mathbf{K} = \mathbf{K}_m + \mathbf{K}_b + \mathbf{K}_s = \int \mathbf{B}_m^T \mathbf{D}_m \mathbf{B}_m dA + \int \mathbf{B}_b^T \mathbf{D}_b \mathbf{B}_b dA + \int \mathbf{B}_s^T \mathbf{D}_s \mathbf{B}_s dA \quad (16)$$

Also, the rotational stiffness matrix can be expressed as Eq. (17) and added to Eq. (16).

$$\mathbf{K}_\theta = \Phi Gh \int \mathbf{B}_\theta^T \mathbf{B}_\theta dA \quad (17)$$

where

$$\mathbf{B}_\theta = \left[ \frac{1}{2} \left( N_{ij,s} \mathbf{V}_r^T - N_{ij,r} \mathbf{V}_s^T \right) N_{ij} \mathbf{V}_t^T \right] \quad (18)$$

The selectively reduced integration scheme is used to compute the stiffness matrix, which is useful for avoiding shear locking. Table 1 gives the selectively reduced integration rule for a linear shell strip. The integration rule is given as the product of the number of rows of Gaussian points in the  $\xi$  direction and the corresponding number in the  $\eta$  direction. As shown in Fig. 7, a single strip with 10 interior nodes in the longitudinal direction has 7 spans (or segments) and the numerical integration is carried out within each span.

The reduced integration scheme is useful in evaluating the stiffness of the drilling part of the energy to avoid an over-constrained situation similar to shear locking (Kebari and Cassell 1991, Choi *et al.* 1999). However, the reduced integration for the drilling part may invoke 5 spurious zero-energy modes, and thus cause a singularity problem when the strips are coplanar. On the other hand, the strip formulation using selectively reduced integration in this study gives almost the same result irrespective of the integration rule used for the drilling part. Therefore, in order to minimize the spurious zero energy modes, the reduced integration is adopted only for computing the shear stiffness.

The number of zero energy modes invoked by the reduced integration is reduced to one by the selective integration of the shear part. However, this mode is non-communicable, and therefore this mode can be removed when at least two strips are used (Cheung and Au 1995).

#### 4. Diaphragm and constraint equation

A box girder bridge has generally high flexural and torsional rigidities. As the box girder is

Table 1 Integration rules

Stiffness	Membrane stiffness	Bending stiffness	Shear stiffness	Drilling stiffness	Zero energy modes
Selectively reduced	2 × 4	2 × 4	1 × 3	2 × 4	1

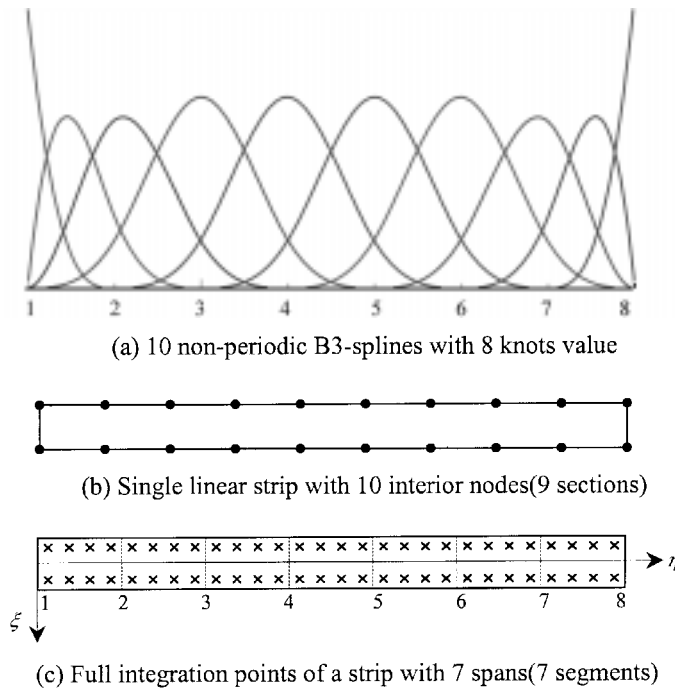


Fig. 7 Numerical integration points of strip

formed by the assembly of thin-walled sections which are rather weak in resisting distortion, a special stiffening system such as a truss, frame, or solid diaphragm is required at sections subjected to large concentrated loads such as at supports.

The stiffening system is normally assumed to be perfectly rigid in its own plane for simplicity and the effect of diaphragms is considered by the penalty method which uses rigid motion of nodes. In this method, one of the nodes in the diaphragm is selected as the master node (Fig. 8) and displacements of all other nodes (slave nodes) are constrained by the master node displacement (Eq. 19). In Fig. 8, the local coordinate ( $r_d, s_d, t_d$ ) axes are defined in the diaphragm and the stiffness matrix and load vector of the diaphragm should be transformed from the global axis into the local axis at supports, because supports are locally restrained.

Then, constraint of each node in the local coordinates is given as follows:

$$\begin{Bmatrix} u_r \\ u_s \\ \theta_t \end{Bmatrix}_{\text{Slave}} = \begin{bmatrix} 1 & 0 & \Delta y_d \\ 0 & 1 & \Delta x_d \\ 0 & 0 & 1 \end{bmatrix} \begin{Bmatrix} u_r \\ u_s \\ \theta_t \end{Bmatrix}_{\text{Master}} \tag{19}$$

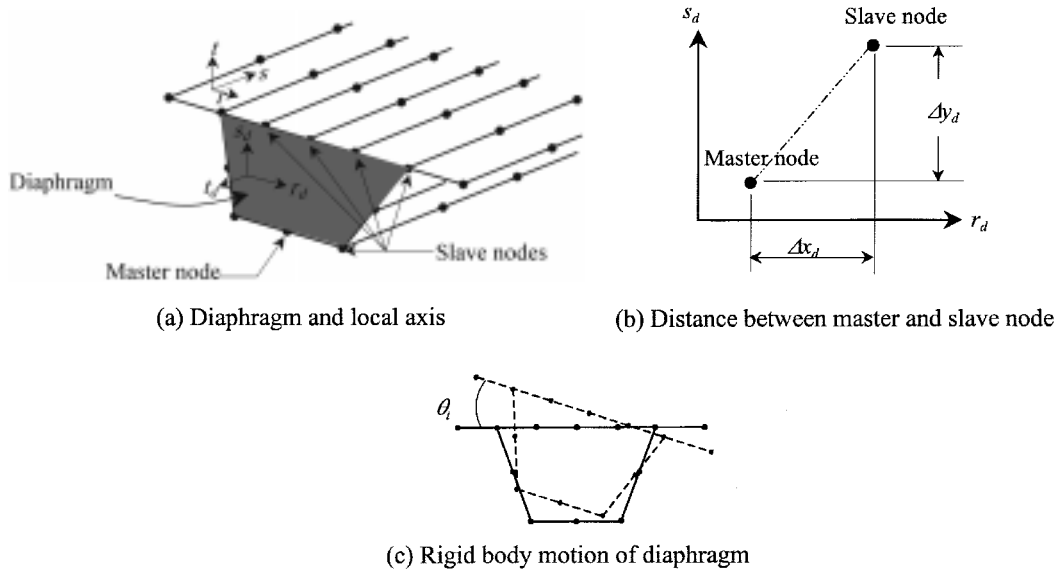


Fig. 8 A support with a diaphragm constraint

Finally, the total stiffness matrix of a strip considering the skew (local) boundary and diaphragms are represented as follows

$$\bar{\mathbf{K}} = \mathbf{T}^T \mathbf{K} \mathbf{T} + \alpha \mathbf{C}^T \mathbf{C} \tag{20}$$

where,  $\mathbf{K}$  is the stiffness matrix of the shell, which does not consider the skew boundary, and  $\mathbf{T}$  is a transformation matrix considering the local axes at the skew boundary.  $\mathbf{C}$  is a constraint equation which is derived from Eq. (19) (Cook 1989) and  $\alpha$  is a penalty coefficient. When the diaphragm has an infinite in-plane stiffness,  $\alpha$  is also infinite. This may properly represent the simply supported condition.

## 5. Numerical examples

### 5.1 Meyer's curved box girder

Fig. 9 shows Meyer's curved box girder with inclined webs (Meyer 1970). This bridge has a 250 ft radius of curvature over the outer web and the rotation angle is 22.92°. The curved girder of Fig. 9(b) is simply supported and the girder is subjected to a single concentrated load of 1.0 kip at midspan over the outer web. Fig. 9(c) illustrates a two-span continuous bridge subjected to self-weight. For the analysis model for the spline FSM, the box girder is divided into 14 strips in the transverse direction and 20 equally-spaced sections in the longitudinal direction. In the case of the single-span bridge, the rigid diaphragms are modeled as simply supported ends, where no vertical movements are permitted. However, in the case of the two-span bridge, the penalty method is introduced in which the rigid motion of the diaphragm is used as a constraint. These constraints are

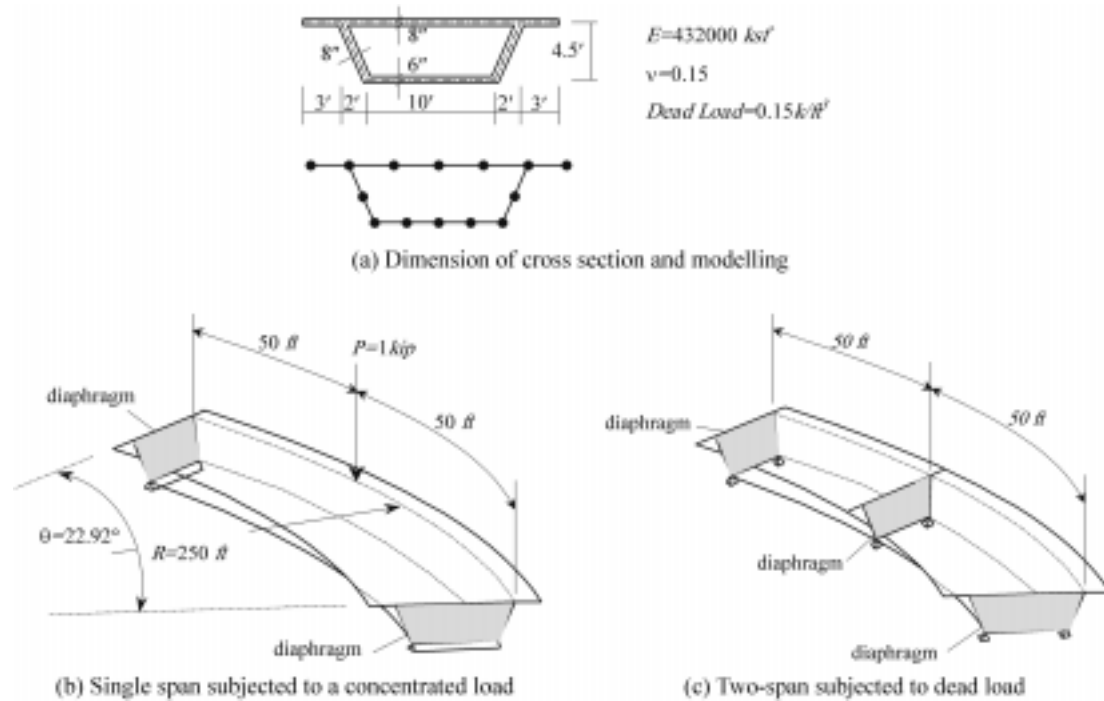


Fig. 9 Meyer's curved box girder bridge

defined in a local coordinate system that is set up in a diaphragm. The non-periodic B3-spline series shown in Fig. 2(b) is used to construct the displacement field and the geometry of shell in all cases. In the model of a commercial FEM program, SAP 2000, used in this study for comparison, the same discretization as the FSM is used in the transverse direction while 60 elements are used in the longitudinal direction.

In Fig. 10 and Fig. 11, the longitudinal resultant membrane forces from the present method are compared with those from SAP 2000. The spline FSM proposed in the current study gives a greater peak value at the support because the modified B-spline series in Fig. 2(b) can pick up the peak value while the FEM may not. Also, membrane force in the mid-section of the bridge shows a good agreement with reference values of Meyer (Fig. 12).

### 5.2 Three-span variable depth curved box girder bridge (Au and Cheung 1996)

A three-span bridge of a variable depth box girder is shown in Fig. 13. The span length is measured along the center line of the bridge. The soffit lines are parabolic with vertical axes. The horizontal alignment consists of a circular curve in the central span and two straight tangents in the end spans. The cross section at an interior support and at the middle of the central span are shown in Fig. 13. A 45 units of abnormal vehicle HB loading to BS5400 was applied at maximum eccentricity on the bridge deck. For the detailed loading conditions, refer to Au and Cheung's work (1996).

Unlike the periodic isoparametric spline FSM in which the bridge is divided into three substructures to achieve an exact geometric model, the non-periodic B3-spline method in this study

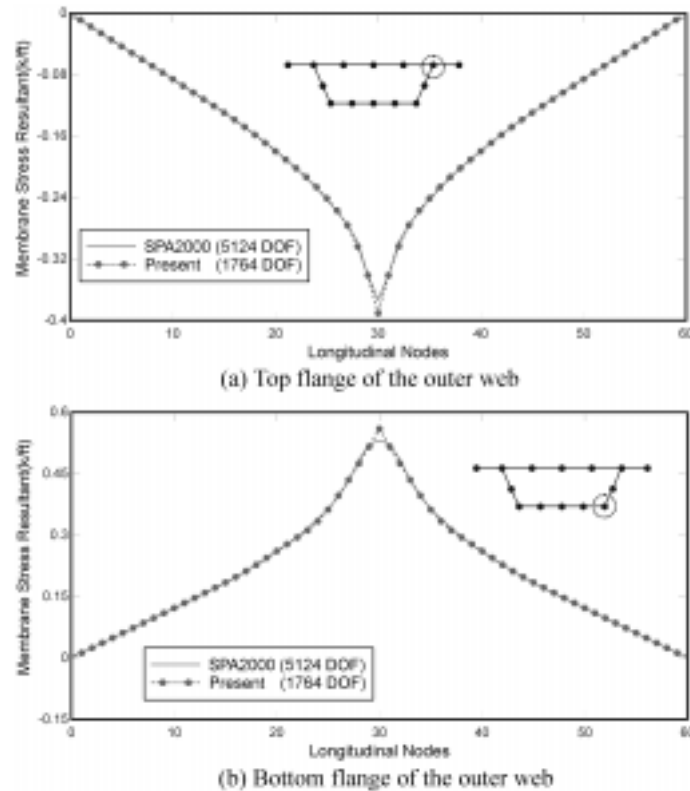


Fig. 10 Membrane force along the bridge length under point load (single span)

uses an assembly of 12 strips each of which extends along the entire bridge length with 24 sections (1800 DOFs). The reference solution was obtained from COSMOS/M (1992), using a 9-node finite element, with 5160 DOFs (Cheung 1996). The deflections at the tips of side cantilevers and the top flange-web junctions at mid-span positions are given in Table 2. The vertical deflections at the tips of the side cantilevers are also presented in Fig. 14. Good agreements are observed.

## 6. Conclusions

The box girder bridge is one of the types of structure to which the finite strip method can be most effectively applied. The special geometry of the box girder, which has a long dimension along the bridge axis and relatively small uniform width and depth (or variable depth), enables us to make the maximum use of the finite strip method in modeling and analysis of the bridge.

The peak negative moments occur at the supports of a multi-span girder due to the reaction acting on the girder and it is very important to obtain an accurate solution. The use of the modified FSM in this study may be the most suitable way to cope with the problem as the modified FSM uses the non-periodic B-spline function which generates the shape function which can well represent the peak value at the boundary. This feature is particularly desirable to pick up the peak value of solution and at the same time satisfy the Kronecker delta property. The results obtained by the

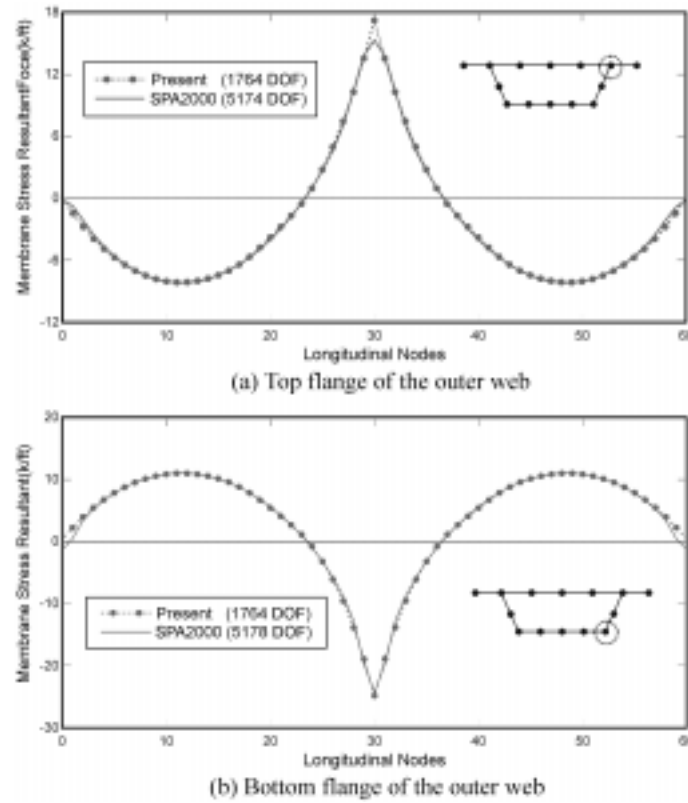
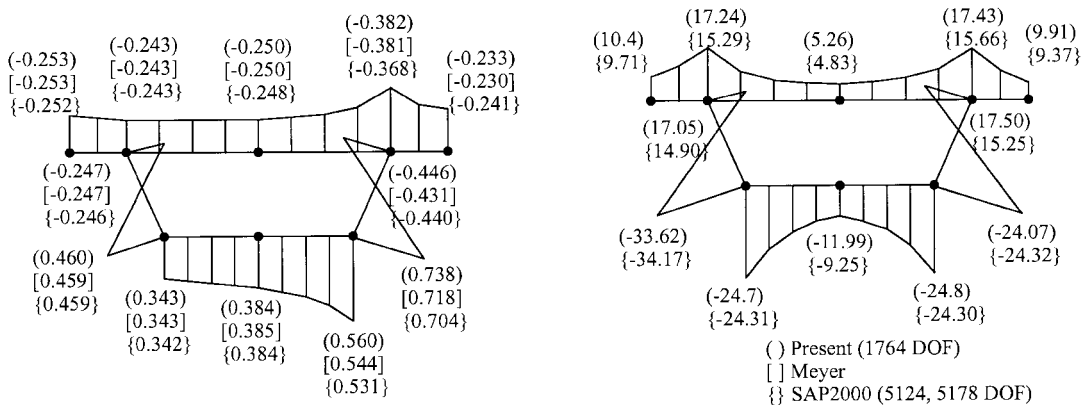


Fig. 11 Membrane force along the bridge length under self weight (two-span)

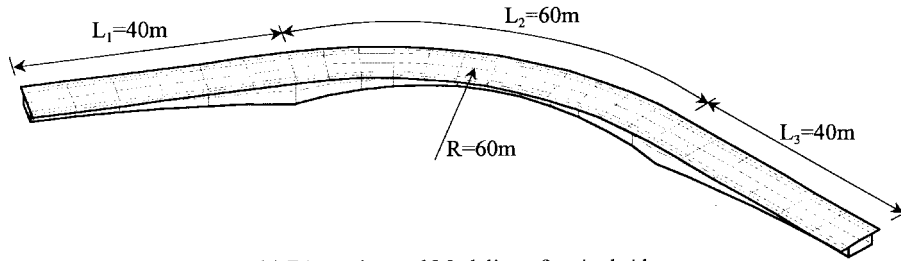


(a) Single span subjected to a concentrated load

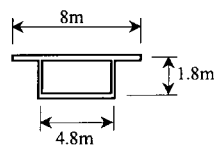
(b) Two-span subjected to dead load

Fig. 12 Membrane force in the mid-section of bridge

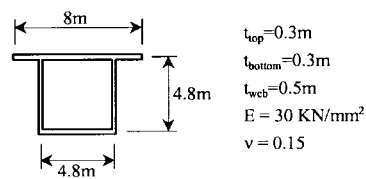
modified FSM in this study are in good agreement with the reference values, even though the total number of DOF used is only about one third that of commercial finite element programs. The use of non-periodic B3-splines provides a highly efficient tool for multi-span bridge analysis, which also



(a) Dimension and Modeling of entire bridge

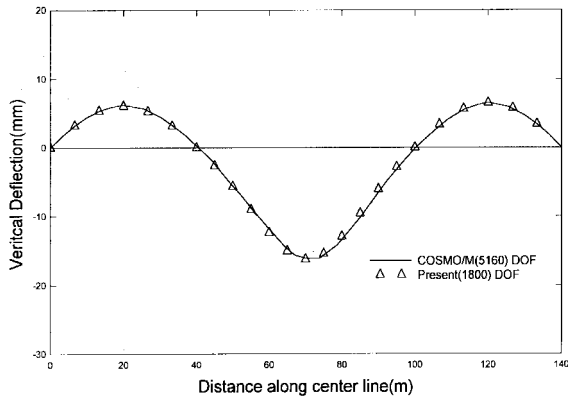


(b) Mid-span section of central span

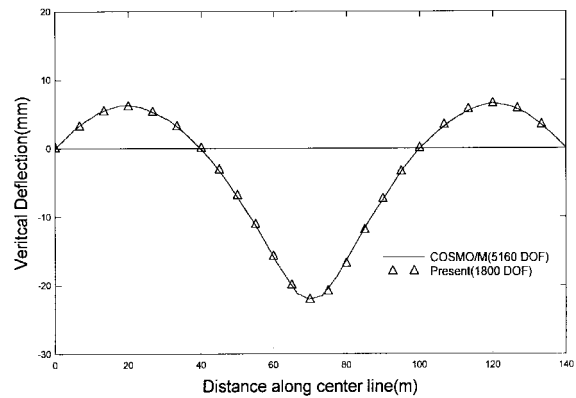


(c) Section at interior support

Fig. 13 Three span variable depth curve box girder bridge



(a) Inner side



(b) Outer side

Fig. 14 Vertical deflection at the tips of side cantilevers

Table 2 Deflection of top flange at mid-span positions (mm)

Position	Method	Tip of left side cantilever	Left flange-web junction	Right flange-web junction	Tip of right side cantilever
Mid-span1	Present	-6.077	-6.048	-6.046	-6.078
	COSMO/M	-6.188	-6.155	-6.155	-6.184
Mid-span2	Present	22.094	20.576	17.305	16.235
	COSMO/M	22.633	21.124	17.579	16.517
Mid-span3	Present	-6.527	-6.494	-6.493	-6.524
	COSMO/M	-6.459	-6.424	-6.402	-6.431

gives better accuracy of solution.

The diaphragms at the interior supports of a multi-span bridge can be treated as a rigid body in the local axis of the diaphragm by introducing the condition of no relative displacements as a penalty constraint. This represents more accurately the simply supported condition, and this concept can be expanded to include interior flexible diaphragms, where the relative displacements are permitted, in a future study.

## References

- Au, F.T.K., and Cheung, Y.K. (1996), "Static and free vibration analysis of variable-depth bridges of arbitrary alignments using the isoparametric spline finite strip method", *Thin-Walled Structures*, **24**, 19-51.
- Chen, C.J., Gutkowski, R.M., and Puckett, J.A. (1991), "Spline compound strip analysis of folded plate structures with intermediate supports", *Comput. and Struct.*, **39**(3/4), 369-379.
- Cheung, Y.K., and Fan, S.C. (1983), "Static Analysis of right box girder bridges by spline finite strip method", *Proc. of the Inst. of Civil Engineers*, Part 2, 75, June, 311-323.1.
- Cheung, Y.K., and Au, F.T.K. (1995), "Isoparametric spline finite strip for degenerated shells", *Thin-Walled Structures*, **21**, 65-92.2.
- Choi, C.K., and Paik, J.G. (1994), "An efficient four node degenerated shell element based on the assumed covariant strain", *Struct. Eng. and Mech.*, **2**(1), 17-34.
- Choi, C.K., Lee, P.S., and Park, Y.M. (1999), "High performance 4-node flat shell element: NMS-4F element", *Struct. Eng. and Mech.*, **8**(2), 209-234.
- Choi, C.K., and Hong, H.S. (2001), "Assumed strain finite strip method using the non-periodic B-spline", *Struct. Eng. and Mech.*, submitted.
- Cook, R.D. (1989), *Concepts and Applications of Finite Element Analysis*, John Wiley & Sons., New York.
- Farin, G. (1992), *Curves and Surfaces for Computer Aided Geometric Design A Practical Guide*, Academic Press.
- Faux, I.D., and Pratt, M.J. (1981), *Computational Geometry for Design and Manufacture*, Ellis Horwood.
- Hoshek, J., and Lasser, D. (1989), *Fundamentals of Computer Aided Geometric Design*, Wellesley, Massachusetts.
- Kebari, H, and Cassell, A.C. (1991), "Non-conforming modes stabilization of a nine-node stress-resultant degenerated shell element with drilling freedom", *Comput. & Struct.*, **40**(3), 569-580.
- Lashkari, M. (1992), *COSMOS/M User Guide*, 7th edn. Structural Research and Analysis Corporation
- Lim, C.G. (1999), "A universal parametrization in B-spline curve and surface interpolation", *Computer Aided Geometric Design*, **16**, 407-422.
- Meyer, C. (1970), "Analysis and design of curved box girder bridges", SESM Report No. 70-22, Department of Civil Engineering, University of California at Berkeley.
- SAP 2000 (1998), *Analysis Reference*, Computers & Structures Inc.
- Uko, C.E.A., and Cusens, A.R. (1988), "Application of spline finite strip analysis to variable depth bridges", *Communications in Applied Numerical Methods*, **4**, 273-278.